THE SEASONAL BEHAVIOR OF WATER ICE CLOUDS IN THE THARSIS AND VALLES MARINERIS REGIONS OF MARS: MARS ORBITER CAMERA OBSERVATIONS. J. L. Benson[1], B. P. Bonev[1], P. B. James[1], K. J. Shan[1], B. A. Cantor[2], and M. A. Caplinger[2], [1]Ritter Astrophysical Research Center, Dept. of Physics and Astronomy, Univ. of Toledo, Toledo, OH 43606 (jbenson@physics.utoledo.edu; bbonev@kuiper.gsfc.nasa.gov; pbj@physics.utoledo.edu), [2]Malin Space Science Systems, P. O. Box 910148, San Diego, CA 92191 (cantor@msss.com; mc@msss.com).

Introduction: Clouds in the martian atmosphere have been observed and studied for many decades. Nathaniel E. Green first identified clouds in the martian atmosphere in 1877 when he observed white spots near the limb of the planet and concluded that they were morning and evening clouds high in the atmosphere [1]. The Tharsis region is known for the "W" clouds [2], which are prominent from northern midspring to midsummer. Smith and Smith [3] studied the diurnal and seasonal behavior of the clouds associated with Olympus Mons using ground based data collected between 1924 and 1971 and found that cloud activity was generally confined to late spring and early summer seasons in the northern hemisphere. Based on a comparison of their data with seasonal water abundances, Smith and Smith concluded that Type I discrete white clouds are composed of water ice. Curran et al. [4] gave the first spectroscopic evidence confirming the presence of water ice clouds on Mars in the Tharsis region using data collected with the infrared interferometer spectrometer on the Mariner 9 spacecraft. The Mariner 9 spectral shape was consistent with a mean radius of the water ice particles of ~ 2.0 μm.

There are several meteorological factors that may contribute to cloud formation and seasonal variability in the Tharsis region. The seasonal variation in the cross-equatorial Hadley cells that characterize the general circulation of the martian atmosphere is an important factor [5]. The local circulation over the volcanoes is also an important factor: low thermal inertia causes the volcanoes to act as a heat source in the atmosphere, and warm upslope winds in the afternoon favor cloud formation and enhance clouds [6]. Insolation and water vapor concentrations are also potentially important factors.

Mars Global Surveyor (MGS) provides the first complete data set with which to study the properties and seasonal variability of clouds throughout the entire martian year. MGS instruments do not provide much diurnal coverage in the equatorial regions, however, because the orbit is fixed at ~ 2pm at the nadir. Only the early afternoon part of the cycle, in which previous observations have suggested growth in the large cloud features, can be studied, but this does make it possible to determine the seasonal behavior, augmented by limited local time coverage.

The Mars Orbiter Camera (MOC) was used to obtain global maps of the Martian surface. The maps used were acquired between March 15, 1999 (L_S = 110º) and July 31, 2001 (L_S = 205º), corresponding to approximately one and a quarter martian years. In this work we focused on water ice clouds associated with the surface features of Olympus Mons, Ascraeus Mons, Pavonis Mons, Arsia Mons, Alba Patera, and the Valles Marineris canyon system. Using these data, we have made three types of quantitative measurements to characterize the cloud activity: 1) cloud area and location, 2) cloud height, and 3) cloud optical depth. We have also searched for short period variations in the cloud areas.

MOC Observations: MOC includes two wide-angle (WA) cameras, one in the blue (400-450 nm) bandpass and the other in the red (575-625 nm) bandpass, each with a 140º field of view [7]. This coverage is optimal for separating clouds that are composed of condensates from those that contain dust; while dust clouds and ice clouds often appear of similar brightness in red, condensate clouds are very bright in blue while dust clouds are dark. The WA camera images are bounded by the horizons, corresponding to nominal local times of 1217 to 1543 at the equator.

A variable summing algorithm is used to obtain continuous observations with both WA cameras so that in a 24-hour period a complete global map is obtained at a resolution of approximately 7.5 km/pixel. To construct the global map, only roughly the center half of each orbital swath's coverage is used; every two hours a new image strip is acquired and added to the previous strips. The daily global maps (DGMs) that we have used for this work are composite cylindrical projections colored with a false green channel.

Cloud Area Measurements: Clouds were identified by visual inspection of the DGMs, and then these features were matched with the blue images taken by MOC. The clouds appear more prominent in blue images due to the relatively high single scattering albedo (~0.9) of these particles relative to the low surface albedo at these wavelengths. To measure the areas of the clouds an IDL program was used, and it took a subset of each DGM that corresponded to the particular surface features studied and measured the number of pixels in the blue image which had a threshold digital number value greater than 120. This value was cho-

sen through visual inspection of cloud boundaries in the blue images. Because the resolution varies with latitude for a cylindrical projection, each line is multiplied by a correction factor. These lines were then added and multiplied by the resolution of the projection at the equator to give the true cloud area.

Cloud Area Results: A plot of cloud area vs. L_S for Olympus Mons is presented in Figure 1. The cloud area maximum near L_S = 100º is likely due to cooler atmospheric temperatures and maximum upward advecting velocities in the solstice Hadley circulation. The cloud area decrease at L_S = 120º is probably caused by the rise in air temperature due to the season (moving away from aphelion) and increased atmospheric dust [8].

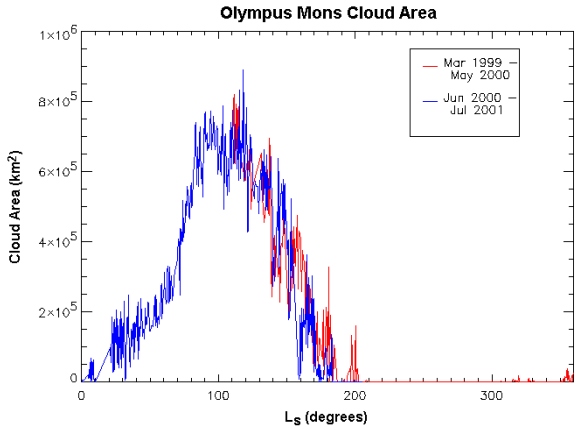

Figure 1: Olympus Mons cloud area versus L_S.

Observations of Ascraeus Mons show the same general trend for cloud area as Olympus Mons, with a peak near L_S = 100º. At L_S = 140º, there is a minimum in cloud area that is especially prominent in the first martian year of observations.

Alba Patera cloud activity displays a double peak feature that was not observed in any of the other regions. The peaks occur at L_S = 60º and 140º, with a minimum near L_S = 85º. The peaks in the seasonal activity of Alba Patera occur at the times that the cloud areas associated with Olympus and Ascraeus Mons volcanoes are rapidly increasing or decreasing; this anticorrelation is one of the most interesting and unexpected results of this study.

Clouds over Pavonis Mons have maximum area near L_S = 100º. There is a local minimum in cloud area at L_S = 140º observed during both martian years. Then cloud area increases for a second peak between L_S = 140º-220º, which corresponds to the time of maximum cloud area at Arsia Mons.

Cloud area vs. L_S for Arsia Mons is shown in Figure 2. Observations of Arsia Mons reveal more or less continuous cloud activity. The only period of inactivity is between L_S = 227º-235º, which corresponds exactly to the largest regional dust storm seen by [8] and [9]. TES observations showed that the dust storm expanded into the region around Arsia Mons at L_S = 228° and was accompanied by a roughly 15 K increase in temperature. By L_S = 237º the dust storm had migrated much further south of Arsia, and the atmospheric temperature in the region had decreased. Richardson et al. [10] demonstrated that cloud ice content decreases strongly as a function of increasing dust optical depth. The temperature increase lowers the relative humidity, suppressing cloud activity [11].

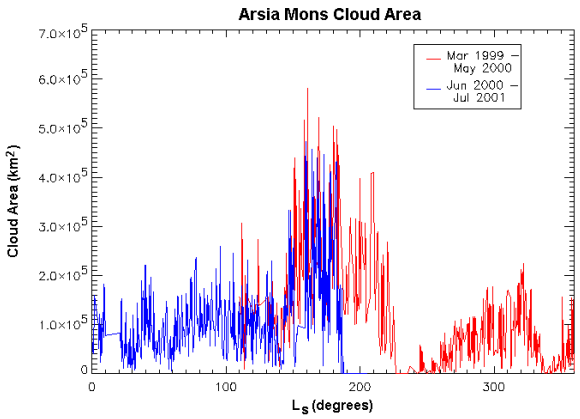

Figure 2: Arsia Mons clouds area versus L_s. Note that the abrupt disappearance of clouds near L_s = 185º is due to the global dust storm of 2001, not to a lack of data.

Cloud activity ends earlier at all of our sites in the second martian year than in the first. This is most clearly seen in Fig. 2. In the first martian year, cloud activity ceased near L_S = 210º at Alba Patera, Olympus Mons, and Ascraeus Mons, and near L_S = 220º at Pavonis Mons. However, in the second martian year, clouds disappeared in all regions between L_S = 183º and L_S = 190º (June 24 and July 4, 2001). This earlier cessation of cloud activity almost certainly results from the global martian dust storm of 2001. As seen from the TES data, atmospheric temperatures near the Tharsis region began to rise around June 25 and the dust storm had expanded into the region by July 2 [12]. As noted above, the increased dust and atmospheric temperature promote the dissipation of water ice clouds.

Valles Marineris: Clouds associated with the western Valles Marineris canyon system and other small surface features were also observed during the time period of this study. The clouds associated with Valles Marineris generally were located in the latitude range -4° to +4° N and longitude range 70° to 80° W. Clouds were also seen around 12° S latitude, 100° W

longitude, in the region of Syria Planum, near 27° N latitude, 107° W longitude, near Ceraunius Fossae, at 26° N latitude, 93° W longitude, surrounding Uranius Patera, and near 30° N latitude, 75° W longitude, not associated with a particular surface feature. Figure 3 shows the location of cloud centers in this region binned into four seasonal bins. Figures 3A and B show numerous clouds in this region during spring and summer, however C and D indicate very few clouds during the fall and winter seasons.

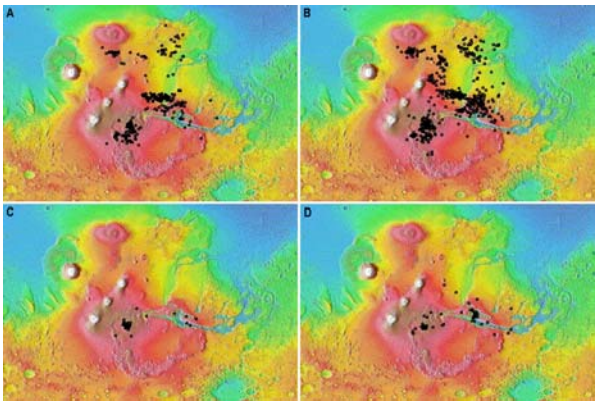

Figure 3: Cloud center locations for Valles Marineris canyon system and other small surface features. (A) L_s = 0º-90º, (B) L_s = 90º-180º, (C) L_s = 180º-270º, (D) L_s = 270º-360º. The background image used is the MOLA topography map of the Tharsis and Chryse region (supplied courtesy of MOLA Science Team).

Cloud Heights: Cloud heights have been determined for each of the five volcanoes for several days throughout their cloudy season. The heights were estimated by visual inspection of the cloud at its highest point of contact with the volcano on the daily global maps. This location was compared to a contour map for each volcano. The elevation of the highest point of contact determined from the contour map was estimated to be the height of the cloud. Cloud heights lie between 19.0-21.0 km for Olympus Mons, 15.0-18.0 km for Ascraeus Mons, 12.0-14.0 km for Pavonis Mons, 16.0-17.4 km for Arsia Mons, and 5.5-6.5 km for Alba Patera. Cloud height error, which depends on the resolution of the contour maps, is estimated at ± 0.5 km for Olympus Mons and ± 1 km for Alba Patera, Ascraeus, Pavonis and Arsia Mons.

From this study of cloud heights, we were able to determine a diurnal correlation; however, no significant seasonal trend was seen. Clouds tended to be at a higher altitude later in the afternoon. On consecutive days, the cloud height could vary 1-2 km depending on local time at the topographic feature. This is consistent with increased convective uplift due to surface heating.

The lower elevation of the Alba clouds is consistent with other unique features: Alba has much lower relief, it is located outside of the ECB (and Hadley uplift) zone, and the seasonal variation of its clouds is unique. The cloud elevation data reinforce the evidence that suggests that the physics of the Alba clouds is different from the clouds in the Tharsis region.

Optical Depth Measurements: Cloud optical depths were calculated for the center coordinate of clouds observed in 154 MOC WA blue filter images using the discrete ordinate, multiple scattering radiative transfer (DISORT) code of Stamnes et al. [13]. We adopt the three layer atmospheric model that has been used extensively in modeling previous HST observations of Mars [14, 15, 16].

The model computed the radiance along 16 streams, and the three layers used correspond to altitude ranges of 0-10, 10-20, and 20-50 km. The relative distribution among the layers for clouds was taken from [17], and we used the single scattering phase function derived by [18]. We adopt a value of 1.0 for the single scattering albedo of clouds [18], and the opacity is specified for a three-layer atmosphere as described in [16].

DISORT was used to calculate the relative cloud optical depth using a region outside the cloud as a reference point. The local cloud optical depth was treated as a free parameter and was varied to get a consistent match with the model. For this calculation, only clouds appearing near the center of the image strip (~1400 LT) were used so that the cosine of the emission angle was greater than 0.50.

In general, the optical depth of clouds in the first Martian year of our observations is smaller than that of the second year, except for Alba Patera, where the optical depths are similar. Optical depth values are found to lie between 0.107-1.015 for Olympus Mons, 0.101-1.358 for Ascraeus Mons, 0.163-1.330 for Pavonis Mons, 0.080-0.820 for Arsia Mons, 0.158-0.753 for Alba Patera, and 0.121-1.10 for Valles Marineris. Results obtained with this technique depend on the surface albedo of the reference point in the range at 425 nm. The surface albedo in the Tharsis region was taken here to be 0.035 [19]. We estimate a possible 15% error due to this choice. Other uncertainties, such as those for the ice and dust single scattering albedo and the calculation of the DN value, are estimated to add another ± 10% uncertainty to the optical depths.

Using the optical depth measurements, H_2O column abundances were calculated. The optical thick-

ness of a cloud, for the thin cloud case, can be approximated by $\tau = NC_{ext}$, where N is the column number density and C_{ext} is the extinction cross section of the ice particle. The mass of H_2O ice in a vertical column per unit area is $m = (4/3)\pi r^3(\tau/C_{ext})\rho$, where r is the mean ice particle radius, and ρ is the mass density of ice. We assumed a mean ice particle radius r = 2 μm. The value used for the extinction cross section, at a wavelength of 0.4 μm, is 20.279 μm^2. The water ice content generally ranges from 0.5 to over 2 pr μm depending on the region.

Afternoon Cloud Variability: The strong diurnal dependence of the clouds associated with the major topographic features has been well documented [3, 20]. These clouds intensify in both size and thickness as the day progresses, reaching maximum extent in the mid- to late afternoon.

MOC images have a fixed nadir of 1400 LT, so the complete cycle of diurnal variations cannot be observed. However, because the orbital period of MGS is not commensurate with the rotation period of Mars, the location of a feature fixed with respect to the Martian surface oscillates on a MOC image relative to the central nadir position on consecutive passes over the feature. The local time at the particular feature also oscillates because it is a function of the position on the image strip. As a result, a continuous series of cloud area measurements covers local times spanning roughly 3.5 afternoon hours – the part of the diurnal cycle generally associated with fast changes of the cloud area. MOC observations have shown that the volcano clouds tend to brighten and increase in area as well as height from early to mid-afternoon.

Quasi-Periodicities of a Short Time Scale: In addition to the seasonal behavior, we examined the evidence for short-term quasi-periodic variability in the cloud areas. The only significant periodicity found gives possible indirect evidence for the afternoon cloud variability discussed above. Unambiguous evidence for periodicities of several sols was not found.

Acknowledgements: Four of the authors (JLB, BPB, PBJ, and KJS) were supported by grants from the Mars Data Analysis Program. BAC and MAC were supported by JPL Contract NAS-7-918.

References: [1] Kieffer, H. H. et al. (1992) In *Mars*, 1-33. [2] Slipher, E. C. (1962) *The Photographic Story of Mars*. [3] Smith, S. A. and Smith, B. A. (1972) *Icarus*, 16, 509-521. [4] Curran, R. J. et al. (1973) *Science*, 182, 381-383. [5] Pollack, J. B. et al. (1993) *JGR*, 98, 3149-3181. [6] Hartmann, W. K. (1978) *Icarus*, 33, 380-387. [7] Malin, M. C. et al. (1992) *JGR*, 97, 7699-7718. [8] Smith, M. D. et al. (2001) *JGR*, 106, 23929-23945. [9] Cantor, B. A. et al. (2001) *JGR*, 106, 23653-23687. [10] Richardson, M. I. et al. (2002) *JGR*, 107, 2-1-2-29. [11] Pearl, J. C. et al. (2001) *JGR*, 106, 12325-12338. [12] Smith, M. D. et al. (2002) *Icarus*, 157, 259-263. [13] Stamnes, K. et al. (1988) *Appl. Opt*., 27, 2502-2509. [14] James, P. B. et al. (1994) *Icarus*, 109, 79-101. [15] Clancy, R. T. et al. (1999) *Icarus*, 138, 49-63. [16] Wolff, M. J. et al. (1999) *JGR*, 104, 9027-9041. [17] Clancy, R. T. et al. (1996) *JGR*, 101, 12777-12783. [18] Clancy, R. T. and Lee, S. W. (1991) *Icarus*, 93, 135-158. [19] Wolff, M. J. et al. (1997) *JGR*, 102, 1679-1692. [20] Hunt, G. E. et al. (1980) *Nature*, 286, 362-364.